Static and dynamic structural analysis of a saturated solution of $ZnBr_2$ in water: Anomalous x-ray diffraction and molecular dynamics simulations

G. Löffler
University of Vienna, Institute for Theoretical Chemistry, Theoretical Biochemistry Group, Währingerstraße 17/Parterre, A-1090 Wien, Austria

Th. Mager
Universität Stuttgart, Institut für Physikalische Chemie, Pfaffenwaldring 55, D-8000 Stuttgart, Germany

Ch. Gerner and H. Schreiber
University of Vienna, Institute for Theoretical Chemistry, Theoretical Biochemistry Group, Währingerstraße 17/Parterre, A-1090 Wien, Austria

H. Bertagnolli
Universität Stuttgart, Institut für Physikalische Chemie, Pfaffenwaldring 55, D-8000 Stuttgart, Germany

O. Steinhauser[a)]
University of Vienna, Institute for Theoretical Chemistry, Theoretical Biochemistry Group, Währingerstraße 17/Parterre, A-1090 Wien, Austria

(Received 16 October 1995; accepted 24 January 1996)

The supposedly very simple system of a saturated solution of $ZnBr_2$ in water exhibits unusually complex and therefore interesting structural behavior. Motivated by this, Mager did a detailed x-ray diffraction study (Th. Mager, PhD. thesis, Universität Würzburg, 1991), and we performed a long molecular dynamics (MD) simulation—using potential parameters from the general purpose GROMOS force field—of such a solution, which can be grossly characterized by the formula $ZnBr_2 \cdot 3H_2O$. We start by calculating those properties that are directly accessible through the experiment from the MD simulation, in order to validate the physical relevance of the simulation. Seeing that the simulation delivers results that are compatible with those of the experiment, we proceed by analyzing the MD simulation in much more detail according to the static and dynamic structure of the system, thereby gaining insight into the structural behavior of $ZnBr_2 \cdot 3H_2O$ that is very difficult, if at all possible, to get from experimental studies. To this end we use the Voronoi algorithm to define coordination shells around atoms and ions in $ZnBr_2 \cdot 3H_2O$. We study the time averaged as well as the time-resolved geometry and composition of these coordination shells and find that octahedral coordination of Zn^{2+} ions is the dominant geometry in $ZnBr_2 \cdot 3H_2O$, and that these octahedra are remarkably stable (after 1 ns only 10% decayed). We further find evidence for polymerlike Zn^{2+} chains, where O atoms of water and Br^- ions connect the Zn^{2+} ions. © *1996 American Institute of Physics.* [S0021-9606(96)50117-5]

I. INTRODUCTION

The picture drawn of the static structure of the saturated solution of $ZnBr_2$ in water ($ZnBr_2 \cdot 3H_2O$) by experimental techniques ranging from vapor pressure measurements and UV, IR, and Raman spectroscopy to x-ray diffraction differential anomolous x-ray scattering (DAS) and extended x-ray absorption fine structure (EXAFS) experiments can be summarized as follows. Strong complexation,[1] which is sometimes described as a quasicrystalline structure,[2–5] can be considered a fact. The Zn^{2+} ions were on the one hand found to be mostly hydrated[2] ($[Zn(OH_2)_n]^{2+}$) and on the other hand coordinated solely by Br^- ions[1–9] ($[ZnBr_4]^{2-}$). The intermediate coordination ($[ZnBr_2(OH_2)_2]^0$) was also found.[10–13] Regarding the exact geometry of the coordination of the Zn^{2+} ions, there is evidence for tetrahedral coordination[6,8–16] as well as for octahedral coordination.[6,8] Another question is, if the coordinated Zn^{2+} ions exist as distinct entities, or whether they are linked together to polymer species, i.e., chains of coordinated Zn^{2+} ions that are held together by the fact that neighbouring Zn^{2+} ions share one or even more ligands. There is evidence for this polymer species,[6,15,16] but there is also at least one study that could not find them.[9] There are several molecular dynamics (MD) studies of ionic solutions reported in the literature, most notably those by Heinzinger and co-workers,[17–19] who have also performed one of the few MD simulations of an ionic solution in the high-concentration regime that is comparable to this work, namely a 0.9 ps MD simulation of $LiCl \cdot 4H_2O$.[20] We know of no molecular dynamics simulation of $ZnBr_2 \cdot 3H_2O$.

In this work we will present the results of a 2.2 ns molecular dynamics simulation of $ZnBr_2 \cdot 3H_2O$ and compare them mainly to the experimental findings of Mager,[21] who performed anomalous x-ray diffraction experiments of this system. The concentration of this solution was 19.50 mole kg^{-1}. The ratio of the number of water molecules to the number of $ZnBr_2$ units is consequently not exactly 3—as suggested by the name $ZnBr_2 \cdot 3H_2O$—but 2.85. Mager's

a)Author to whom all correspondence should be addressed.

TABLE I. The atom-specific parameters for the Lennard-Jones interaction (See text for details).

Atom type	Partner	$A'/kJ^{1/2}\ \mathrm{mol}^{-1/2}\ \mathrm{nm}^6$	$B'/kJ^{1/2}\ \mathrm{mole}^{-1/2}\ \mathrm{nm}^3$
Zn^{2+}	Zn^{2+},Br^-,O,H	0.9716×10^{-4}	0
Br^-	Zn^{2+},Br^-,O,H	0.1544×10^{-1}	0.132 96
O	Zn^{2+},O,H	0.1623×10^{-2}	0.051 16
O	Br^-	0.8615×10^{-3}	0.047 56
H	Zn^{2+},Br^-,O,H	0	0

main results concerning the static structure of $ZnBr_2\cdot3H_2O$ are as follows. The majority of the Zn^{2+} ions cannot be completely hydrated, because on average there is only one water molecule available per Zn^{2+} ion. Every Zn^{2+} ion is surrounded by an average of 1.6 water molecules and 4.0 Br^- ions. The main symmetry of the coordination of Zn^{2+} ions is a tetrahedron, and most of these tetrahedra are formed by four Br^- ions ($[ZnBr_4]^{2-}$). On the other hand, the existence of a considerable amount of Zn^{2+} ions that are coordinated by two Br^- ions and two water molecules ($[ZnBr_2(OH_2)_2]^0$) can be ruled out. More than 50% of all Zn^{2+} ions participate in polymer species, the rest is hydrated and interstitial. The question, whether these polymer species are chained together to form networks of chains, could not be answered.

II. EXPERIMENTAL RESULTS AND SIMULATED RADIAL DISTRIBUTION FUNCTIONS

We used molecular dynamics[22] to simulate the time development of $ZnBr_2\cdot3H_2O$ for a time period of 2.2 ns. The other characteristics of this MD simulation include the following.

System size $(3.461\ \mathrm{nm})^3$.

The system contained 233 units $ZnBr_2$ and 663 simple point charge (SPC) water molecules,[23] all together 2688 atoms. The resulting concentration of $ZnBr_2$ is 19.51 mole kg^{-1}, which is very close to the experimental concentration of 19.50 mole kg^{-1}.

Temperature: 300 K, held constant with coupling to an external heat bath.[24]

Time step for the integration of the Newtonian equations of motion: 2 fs.

Usage of a constraint algorithm for the maintainance of the geometry of water molecules.[25]

Cutoff for Lennard-Jones interaction: 1.0 nm.

Ewald summation[26–28] for the electrostatic interactions using a decay-parameter $\eta=2.179\,82$, 230 k-vectors and a cutoff for the real part of the Ewald interaction of 1.2 nm.

The spatial extension of atoms was described by the Lennard-Jones potential $U_{\mathrm{LJ}}=A_{ij}/r^{12}-B_{ij}/r^6$, where the pair-specific parameters A_{ij} and B_{ij} were calculated from atom-specific parameters: $A_{ij}=A_i'A_j'$ and $B_{ij}=B_i'B_j'$. These atom-specific parameters were—with the exception of the Br^- parameters—taken from the general purpose force field of the GROMOS package[29] and are summarized in Table I. GROMOS does not give parameters for Br^-, so we derived the Br^- parameters from the known Cl^- parameters.

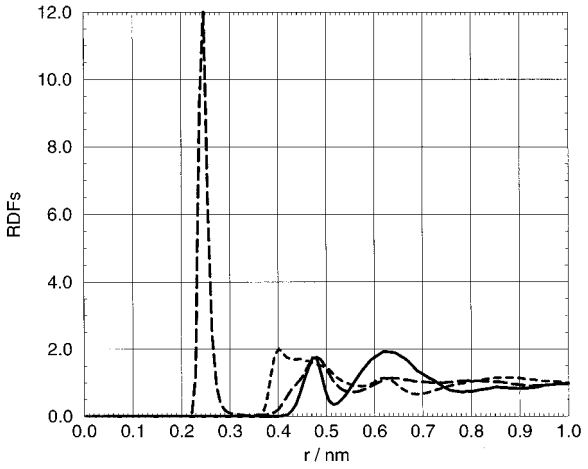

FIG. 1. The simulated radial distribution functions between ions of $ZnBr_2$. g_{ZnZn}, solid line; g_{ZnBr}, long-dashed line; g_{BrBr}, dashed line.

The partial charges on the atoms of water were according to the SPC model[23] $-0.82e$ (on O) and $+0.41e$ (on each H). The charges of Zn^{2+} and Br^- were of course $+2e$ and $-1e$, respectively. The simulation was performed on an SGI Indy with a 100 MHz $R4000$ processor using a homegrown MD program.

The primary result of an MD simulation are the positions and velocities of all the atoms in the system at all the time steps of the MD run. The radial distribution functions (RDF's) of the system can easily be calculated from these sets of positions. They are shown in Figs. 1–3.

Of course, anomalous x-ray diffraction does not deliver the RDF's, but only linear combinations of them. On the other hand, once the RDF's have been calculated from the simulation, they can be linearly combined to reproduce these experimental functions. In this fashion we will compare three experimental functions of the system $ZnBr_2\cdot3H_2O$ as determined by Mager[21] to their simulated counterparts.

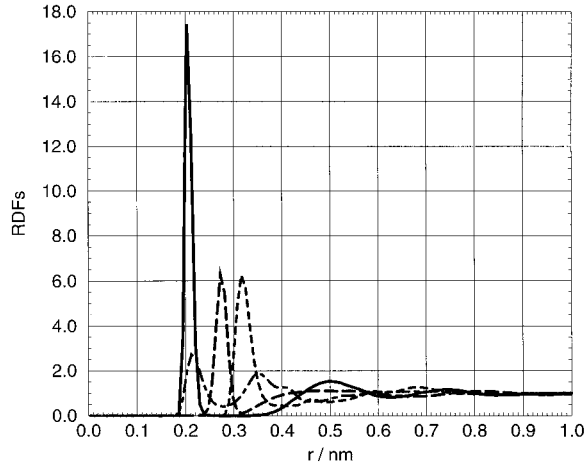

FIG. 2. The simulated radial distribution functions between ions of $ZnBr_2$ on the one hand and atoms of H_2O on the other. g_{ZnO}, solid line; g_{ZnH}, long-dashed line; g_{BrO}, dashed line, g_{BrH}, dotted-dashed line.

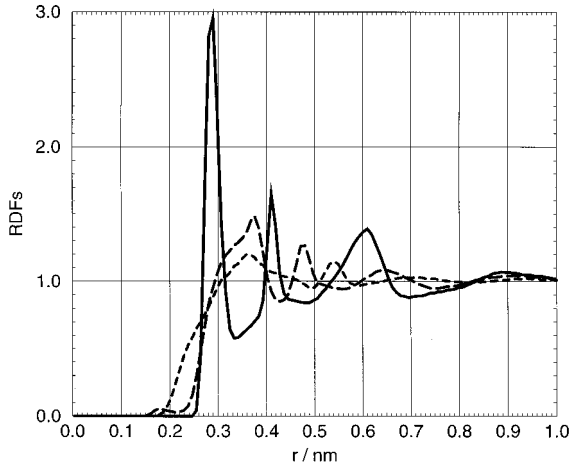

FIG. 3. The simulated radial distribution functions between atoms of H_2O. g_{OO}, solid line; g_{OH}, long-dashed line; g_{HH}, dashed line.

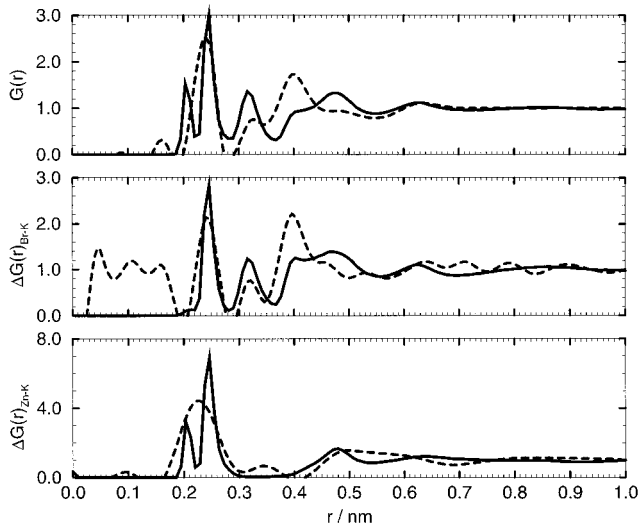

FIG. 4. Total radial distribution function (upper graph), radial difference distribution function at the Br–K absorption edge (middle graph) and radial difference distribution function at the Zn–K absorption edge (bottom graph) as found by simulation (solid line) and experiment (dashed line). The oscillations in the experimental functions at distances smaller than 0.2 nm stem from cutoff effects.

Figure 4 compares the total radial distribution function $[G(r)]$, the radial difference distribution functions at the Br–K $[\Delta G(r)_{\mathrm{Br-K}}]$ and at the Zn–K absorption edge $[\Delta G(r)_{\mathrm{Zn-K}}]$ as determined experimentally[21] and as calculated by linear combination of the simulated RDF's using the coefficients listed in Table II.[21]

$G(r)$: Looking at the first (broad) peak at 0.24 nm in the experimental function we notice that it is resolved into two peaks in the simulated function, which are located at 0.21 and 0.25 nm, respectively. The experimental peak can be regarded as the envelope of the two simulated peaks, because height and position match. The following three peaks (at 0.32, 0.40, and 0.48 nm) can be found at identical positions in the experimental and in the simulated function, although the heights of all three peaks vary considerably between simulation and experiment. In general, peak heights in distribution functions that were determined with anomalous x-ray diffraction underlie a much greater experimental error than peak positions.

$\Delta G(r)_{\mathrm{Br-K}}$: The first peak in both, the experimental and the simulated function, is located at 0.24 nm. The experimental peak at this position is a bit broader, but also a bit smaller than the corresponding simulated peak. The simulated peak at 0.32 nm is in good agreement with the experimental peak at the same position, although the former is a bit higher than the latter. The experimental and simulated peaks near 0.40 nm differ in height.

$\Delta G(r)_{\mathrm{Zn-K}}$: As in the case of $G(r)$, we observe a broad experimental peak near 0.23 nm, which again envelopes the two simulated peaks at 0.21 and 0.25 nm. The experiment shows a small, broad peak at 0.34 nm that is not observed in the simulated function. The peak near 0.48 nm is much broader and stretched in the experiment than it is in the simulation.

All in all, the correspondence in the positions of the peaks in the experimental and simulated functions shown in Fig. 4 is good, whereas the deviations in corresponding peak heights are—not unexpectedly—much larger. Since experiment and simulation were shown to be in reasonable accordance, we are now in a position to provide reliable structural information from the simulation that is not accessible experimentally.

III. COORDINATIONAL ANALYSIS IN TERMS OF VORONOI POLYHEDRA

The strongly and characteristically structured radial distribution functions that we calculated from the molecular dynamics simulation of $ZnBr_2 \cdot 3H_2O$ document the existence of a pronounced short-range ordering of the ions (Zn^{2+}, Br^-) and molecules (H_2O) in this system. First we will describe an algorithm that allows the characterization of the short-range ordering around a central atom, then we will use this algorithm to describe the static (i.e., time averaged) and dynamic (i.e., time resolved) structure of $ZnBr_2 \cdot 3H_2O$.

TABLE II. The linear combination coefficients of the radial distribution functions in the total and difference distribution functions.

Function	g_{ZnZn}	g_{ZnBr}	g_{BrBr}	g_{ZnO}	g_{ZnH}	g_{BrO}	g_{BrH}	g_{OO}	g_{OH}	g_{HH}
$G(r)$	0.050	0.245	0.299	0.082	0.021	0.201	0.050	0.034	0.017	0.002
$\Delta G(r)_{\mathrm{Br-K}}$	0.000	0.232	0.531	0.000	0.000	0.190	0.048	0.000	0.000	0.000
$\Delta G(r)_{\mathrm{Zn-K}}$	0.192	0.576	0.000	0.186	0.046	0.000	0.000	0.000	0.000	0.000

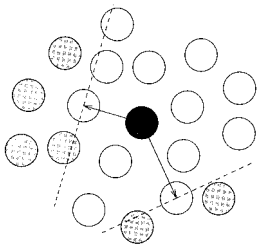

FIG. 5. Two-dimensional illustration of the Voronoi algorithm. The central atom is shown in dark grey, the vector connecting central atom and ligand and the plane perpendicular to this vector (dashed line) are shown for two ligand atoms. The atoms that were ruled not to belong to the first coordination shell based on these two ligand-atoms are shown in light grey.

The atoms (charged or uncharged; in this context often called ligands) surrounding a central atom may be categorized in quasispherical coordination shells, where the first coordination shell is the one closest to the central atom. Given the positions of a central atom and its ligands, how can the ligands be assigned to the first, second, etc., coordination shell? Because the possibility of distortion of the coordination shells from the ideal spherical geometry prohibits the use of a simple distance criterion to discriminate between the shells, we used the Voronoi algorithm[30–32] which can be described as follows (see Fig. 5). For every ligand (i) construct a vector from the central atom to the ligand, (ii) construct a plane perpendicular to this vector going through the center of the ligand, (iii) for every other ligand—if the ligand lies on the other side of the plane than the central atom, this ligand is not a member of the first coordination shell.

After applying this algorithm to a central atom and its surrounding atoms, the atoms being part of the first coordination shell are the only ones that were not marked for exclusion by the algorithm. If the ligands of the second coordination shell are sought, they can be constructed by applying the Voronoi algorithm independently to all atoms of the first shell and uniting all these partial results. The second shell consists of all atoms in this set that are neither members of the first shell nor the central atom itself.

A. Static coordination

In this section we will use the Voronoi algorithm to characterize the static, i.e., time-averaged structure of $ZnBr_2 \cdot 3H_2O$. All properties presented here were averaged over the whole MD trajectory (2.2 ns). The insight from this analysis can directly be applied to the explanation of the main features of the RDF's of this system.

A question that is vividly discussed in the literature[6,9,15,16,21] is whether there exist polymerlike species in $ZnBr_2 \cdot 3H_2O$, i.e., whether Zn^{2+} ions are chained together by either Br^- or O atoms. To answer this question, we constructed the first coordination shell around every O atom and Br^- ion and counted the number of Zn^{2+} ions in this shell. In the case of linearly chained Zn^{2+} ions, we expect that a significant number of O atoms and/or Br^- ions are coordinated by two Zn^{2+} ions. Branched Zn^{2+} chains could be identified by Br^- ions and/or O atoms that are surrounded by three or more Zn^{2+} ions in the first coordination shell. Tables III and IV show the (time-averaged) distribution of the number of Zn^{2+} ions in the first coordination shell around Br^- ions and O atoms, respectively. It can be seen, that 42% of all Br^- ions and 33% of all O atoms are coordinated by only one Zn^{2+} ion and, therefore, either do not participate in any chaining of Zn^{2+} ions or are coordinated to the final Zn^{2+} ion in such a chain. 37% of all Br^- ions and a remarkable 47% of all O atoms bridge two Zn^{2+} ions and thereby form the generic monomer of polymerlike Zn^{2+} chains. A considerable percentage of Br^- ions as well as O atoms are coordinated by three or more Zn^{2+} ions, which suggests that branched Zn^{2+} chains are fairly commonplace in $ZnBr_2 \cdot 3H_2O$. It is also noteworthy, that 6% of all Br^- ions are not coordinated to any Zn^{2+} ion. It seems obvious, that these Br^- ions are purely solvated by water molecules. Altogether, we found evidence for the existence of (partially branched) polymerlike Zn^{2+} chains through the detection of the necessary chain elements. From here on we will restrict the coordinational analysis to the first coordination shell around Zn^{2+} ions. Since the only reasonable ligands of the highly positively charged Zn^{2+} can be ligands bearing a (at least partial) negative charge, we will furthermore require the members of the first coordination shell to be either O or Br^-. The reason that we can ignore the precise coordination geometry of Br^- ions and O atoms is, that Zn^{2+} as the by far highest charged ion in $ZnBr_2 \cdot 3H_2O$ must also act as the main coordinating species. We can also motivate the restriction to the coordination of Zn^{2+} *a posteriori* with the fact, that based on these coordinations alone we were able to explain all major features of the RDF's of $ZnBr_2 \cdot 3H_2O$.

The distribution of the size of the first coordination shell around Zn^{2+} is shown in Table V. We can see that, by far, most Zn^{2+} ions are coordinated by six ligands (which can be either Br^- or O). The distribution of the distances from the

TABLE III. The distribution of the number of Zn^{2+} ions in the first coordination shell around Br^- ions.

No. of Zn^{2+}	% of all Br^-
0	5.5
1	42.2
2	36.5
3	12.3
4	3.0
5	0.3

TABLE IV. The distribution of the number of Zn^{2+} ions in the first coordination shell around O atoms.

No. of Zn^{2+}	% of all O
0	0.0
1	33.4
2	46.7
3	17.5
4	2.2
5	0.1

TABLE V. The distribution of the size of the first coordination shell (i.e., the number of ligands comprising it) around Zn^{2+}.

No. of ligands	% of all Zn^{2+}
0	0.0
1	0.0
2	0.0
3	0.0
4	3.0
5	28.6
6	61.2
7	6.6
8	0.6
9	0.0
10	0.0

central Zn^{2+} ion to the atoms in the first shell is shown in Fig. 6. The two peaks at 0.21 and 0.25 nm can be easily assigned to O and Br^-, respectively. The position of the peaks marking the Zn^{2+}–O distance and the Zn^{2+}–Br^- distance stays the same throughout the following discussion of each of the differently sized coordination shells and will therefore not be mentioned there. The Zn^{2+}–O distance of 0.21 nm and the Zn^{2+}–Br^- distance of 0.25 nm can be regarded as the canonical distances in all coordination shells around Zn^{2+} ions. Almost all first coordination shells are restricted to a spherical region with a radius of 0.32 nm around the Zn^{2+} ions (see Fig. 6), but this does not imply that all atoms within 0.32 nm around a Zn^{2+} ion are part of its first coordination shell! In other words, the Voronoi algorithm could not have been replaced with a simple distance criterion of 0.32 nm. We will now look at each of these differently sized coordination shells in more detail.

1. The 6-atom sized first coordination shell around Zn^{2+}

Table VI shows the distribution of the number of Br^- ions in this shell type. We see that most of these Zn^{2+} ions are coordinated by two Br^- ions and four O atoms. To get an

TABLE VI. The distribution of the number of Br^- ions in the six-atom sized first coordination shell around Zn^{2+}.

No. of Br^-	% of Zn^{2+} with six ligands
0	0.7
1	11.3
2	46.3
3	30.1
4	9.0
5	1.9
6	0.7

idea of the exact geometry of the coordination of a Zn^{2+} ion, the angles formed by a ligand, the central ion and a second ligand can be calculated. In Fig. 7 the distribution of these angles as found at those Zn^{2+} ions that are coordinated by two Br^- ions and four O atoms is shown. In this coordination type, all angles are near 90° or 180°, which is only compatible with an octahedral coordination of the central Zn^{2+} ion. A noteworthy exception are the smaller Br^-–Zn^{2+}–Br^- angles, which lie near 100° rather than 90° and consequently give rise to a slightly distorted octahedron. Zn^{2+} ions surrounded by one Br^- ion and five O atoms show an identical distribution of angles, which is not shown here.

The distribution of angles in the other witnessed coordination types involving six ligands (three Br^- and three O; four Br^- and two O) is increasingly less pronounced than in the cases with one or two Br^- ions (data not shown) which suggests that steric hindrance and electrostatic repulsion between the ligands, in general, and the Br^- ions, in particular, become too strong in these coordination types to permit the formation of a well-defined structure, let alone a regular octahedron.

To formally decide whether a particular polyhedron is of regular geometry (an octahedron in this case), we calculated the average absolute deviation of the angles of the polyhe-

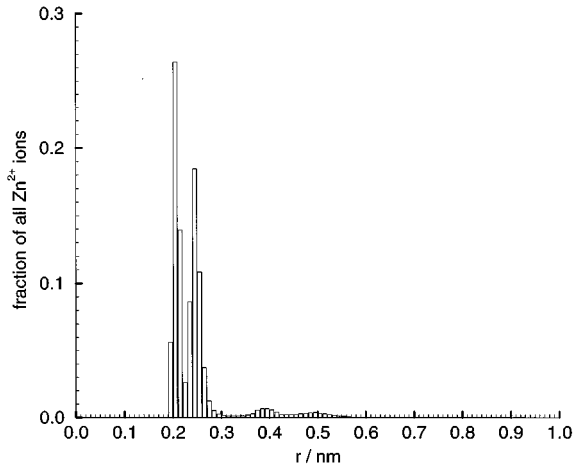

FIG. 6. The distribution of distances from the central Zn^{2+} ion to the ligands of its first coordination shell.

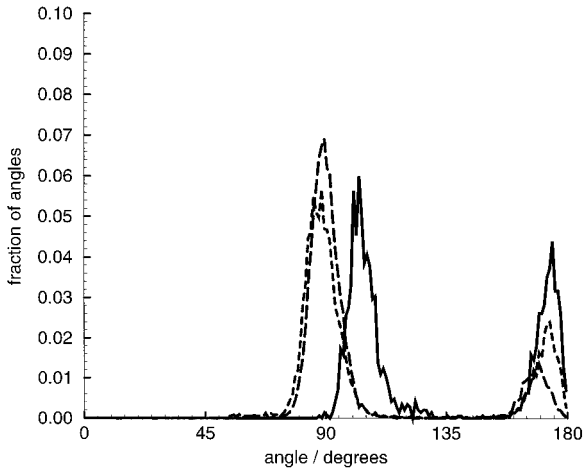

FIG. 7. The distribution of the Br^-–Zn^{2+}–Br^- angles (solid line), Br^-–Zn^{2+}–O angles (long-dashed line), and O–Zn^{2+}–O angles (dashed line) as found in Zn^{2+} ions that are coordinated by two Br^- ions and four O atoms.

TABLE VII. The static distribution of the important coordination types of Zn^{2+}.

Characterization of the coordination type	% of all Zn^{2+}
Four Br^- or O	3.0
Tetrahedron	3.0
Tetrohedron with four Br^-	1.3
Tetrohedron with three Br^-, one O	1.6
Five Br^- or O	28.6
Trigonal Bipyramid	23.0
Trigonal bipyramid with three Br^-, two O	15.8
as above, and O on opposite vertices	15.0
Six Br^- or O	61.2
Octahedron	44.5
Octrahedron with one Br^-, five O	6.9
Octrahedron with two Br^-, four O	26.6
as above, and Br^- on opposite vertices	10.7
Octrahedron with three Br^-, three O	10.5
Octrahedron with four Br^-, two O	0.2
Others	7.3

dron from the angles of the regular structure. If this deviation was less than 10°, the polyhedron was said to have this regular structure.

Using this quantitative criterion, we found that 45% of all Zn^{2+} ions are octahedrally coordinated, whereas the total percentage of Zn^{2+} ions with six ligands is 61% (see Table VII). We also found that 11% of all Zn^{2+} ions (or 24% of all octahedrally coordinated Zn^{2+} ions) are octahedrally coordinated by two Br^- and four O ions, where the two Br^- ions are situated on opposite vertices of the octahedron [see Fig. 8(c)]. This geometry is the prototype of the octahedral coordination of Zn^{2+}.

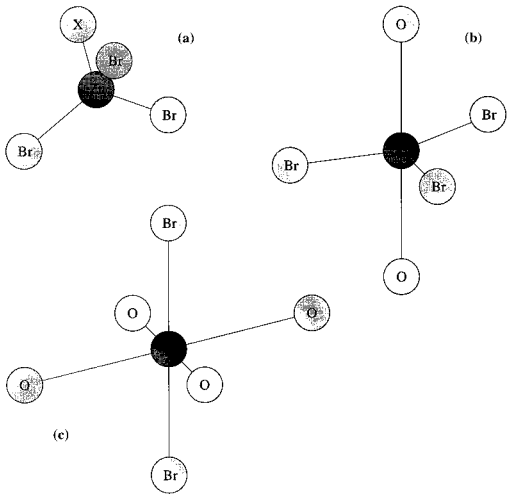

FIG. 8. The typical coordination of Zn^{2+} involving four, (b) five, and (c) six ligands. × denotes either Br^- or O.

TABLE VIII. The distribution of the number of Br^- ions in the five-atom sized first coordination shell around Zn^{2+}.

No. of Br^-	% of Zn^{2+} with five ligands
0	0.0
1	0.3
2	21.2
3	58.9
4	16.9
5	2.8

2. The 5-atom sized first coordination shell around Zn^{2+}

29% of all Zn^{2+} ions are surrounded by five Br^- ions or O atoms (see Table VII). The distribution of the number of Br^- ions in the coordination shells of this kind (Table VIII) shows that the highest fraction contains three Br^- ions and, consequently, two O atoms.

The distribution of the angles for the coordination type with three Br^- ions and two O atoms (Fig. 9) shows a characteristic clustering of Br^-–Zn^{2+}–Br^- angles near 120°, of Br^-–Zn^{2+}–O angles near 90° and of O–Zn^{2+}–O angles near 180°. This is strong evidence for the assumption that the first coordination shell in this case forms a trigonal bipyramid centered at the Zn^{2+} ion. The three Br^- ions thereby form a regular triangle and the two O atoms are positioned at the vertices above and below the plane of this triangle [see Fig. 8(b)].

As summarized in parts of Table VII, we found that 23% of all Zn^{2+} ions are coordinated by a trigonal bipyramid. 69% of these Zn^{2+} ions (or 16% of all Zn^{2+} ions) are surrounded by a trigonal bipyramid made of three Br^- ions and two O atoms and almost all of those (15% of all Zn^{2+} ions) have the geometry shown in Fig. 8(b).

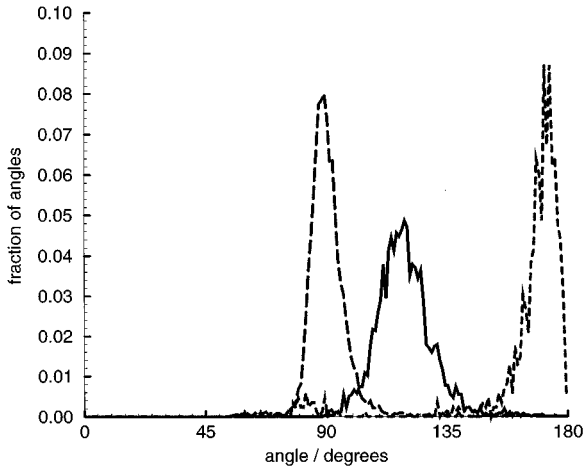

FIG. 9. The distribution of the Br^-–Zn^{2+}–Br^- angles (solid line), Br^-–Zn^{2+}–O angles (long-dashed line), and O–Zn^{2+}–O angles (dashed line) as found at Zn^{2+} ions that are coordinated by three Br^- ions and two O atoms.

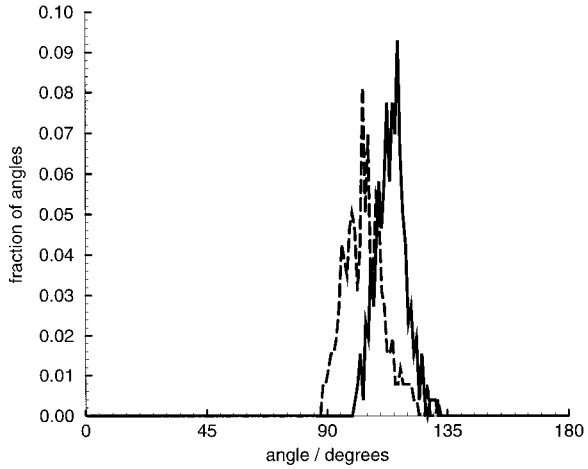

FIG. 10. The distribution of the Br^-–Zn^{2+}–Br^- angles (solid line) and Br^-–Zn^{2+}–O angles (dashed line) as found in Zn^{2+} ions that are coordinated by three Br^- ions and one O atom.

3. The four-atom sized first coordination shell around Zn^{2+}

Although only 3% of all Zn^{2+} ions are surrounded by a first coordination shell made up of four Br^- ions or O atoms (see Table VII), practically all of those shells form a regular tetrahedron. As might be expected from the relatively low number of ligands that make up a tetrahedron, space requirements of the ligands are not a problem in this case. Consequently, the number of (the large) Br^- ions in the tetrahedra can be quite high: 44% of all tetrahedra (1.3% of all first coordination shells around Zn^{2+} ions) are made of four Br^- ions and the remaining 56% (1.6% in all) contain three Br^- ions and one O atom.

Figure 10 shows the distribution of the angles that appear at the Zn^{2+} ions that are surrounded by three Br^- ions and one O atom. Due to the smaller radius of the O atom compared to that of the Br^- ions, the Br^-–Zn^{2+}–O angles are slightly smaller than the Br^-–Zn^{2+}–Br^- angles. However, all of the angles cluster remarkably around the tetrahedral angle of 109.5°. The prototypical tetrahedral coordination of a Zn^{2+} ion is shown in Fig. 8(a).

4. Other coordination shells around Zn^{2+}

All other first coordination shells around Zn^{2+} ions, most notably those containing seven Br^- ions or O atoms, do not show any significantly pronounced structure when analyzed on the basis of the angular distribution (data not shown). Altogether, these unstructured coordinations make up a total of 7% of all Zn^{2+} ions (see Table VII).

5. Explaining the radial distribution functions through the coordination of the Zn^{2+} ions

Using the previously gained insight into the possible coordinations of Zn^{2+} ions in $ZnBr_2 \cdot 3H_2O$—which are characterized by the drawings in Fig. 8 and by the typical Zn^{2+}–O distance of 0.21 nm and the typical Zn^{2+}–Br^- distance of 0.25 nm (see Fig. 6)—we can try to assign peaks in the RDF's of this system to specific distances in the coordination polyhedra. Of course, since the only atoms and ions that took part in our coordinational analysis were Zn^{2+}, Br^-, and O, the only RDF's we can hope to explain are $g_{ZnBr}(r)$, $g_{ZnO}(r)$, $g_{BrBr}(r)$, $g_{BrO}(r)$, and $g_{OO}(r)$. Moreover, because as mentioned earlier, the first coordination shell of Zn^{2+} has a maximum radius of about 0.32 nm, we can only try to explain the short-range part of the mentioned RDFs. The interpretation of these RDF's is as follows.

$g_{ZnBr}(r)$ (Fig. 1). The generic distance from a central Zn^{2+} ion to a Br^- ion in the first coordination shell around this Zn^{2+} ion is 0.25 nm, and this is also the position of the first peak in $g_{ZnBr}(r)$.

$g_{ZnO}(r)$ (Fig. 2). The generic distance from a Zn^{2+} ion to its coordinating O atom is 0.21 nm. This is exactly the position of the first peak in $g_{ZnO}(r)$.

$g_{BrBr}(r)$ (Fig. 1). Let us first have a look at the first peak of $g_{BrBr}(r)$. This peak has a very broad appearance, suggesting that it is actually made of several peaks. The broad peak extends from 0.4 nm to about 0.5 nm and under close examination shows at least two subpeaks: one near 0.4 nm, which is also the highest of these subpeaks, and one near 0.44 nm. Br^-–Br^- distances can be found in any of the three typical Zn^{2+} coordinations. In the tetrahedron, where the Br^-–Zn^{2+}–Br^- angle is 109.5°, the average distance between two Br^- ions is 0.41 nm. This corresponds very well to the first subpeak in $g_{BrBr}(r)$. In the trigonal bipyramid, the Br^-–Zn^{2+}–Br^- angle is 120°, which gives rise to a Br^-–Br^- distance of 0.43 nm. This obviously explains the second subpeak in $g_{BrBr}(r)$, which lies near 0.44 nm. The largest Br^-–Br^- distance in any coordination polyhedron is the one in the octahedron, where the two Br^- ions are situated at opposite vertices. Their distance in this case is 0.50 nm and corresponds closely to the final part of the first peak in $g_{BrBr}(r)$.

$g_{BrO}(r)$ (Fig. 2). Both, in the typical trigonal pipyramid as well as in the typical octahedron, the Br^-–O distance is 0.33 nm. The first peak in $g_{BrO}(r)$ is sharp and well pronounced and lies at 0.32 nm.

$g_{OO}(r)$ (Fig. 3). In the typical trigonal bipyramid, both O atoms are situated at opposite vertices. This results in a separation of 0.42 nm, which is exactly the position of the second peak in $g_{OO}(r)$. In the octahedron there are two possible O–O distances: one is identical to the one found in the trigonal bipyramid, because it involves two O atoms separated by a Zn^{2+} ion; the second distance is described by the O–Zn^{2+}–O angle of 90° and is therefore 0.30 nm. This is very close to the first peak in $g_{OO}(r)$, which is found at 0.29 nm.

We see that by taking into account only the most frequent regular coordination geometries around Zn^{2+} ions and the two canonical distances therein (Zn^{2+}–O, 0.21 nm; Zn^{2+}–Br^-, 0.25 nm), we are able to explain all short-range peaks in the RDF's $g_{ZnBr}(r)$, $g_{ZnO}(r)$, $g_{BrBr}(r)$, $g_{BrO}(r)$, and $g_{OO}(r)$.

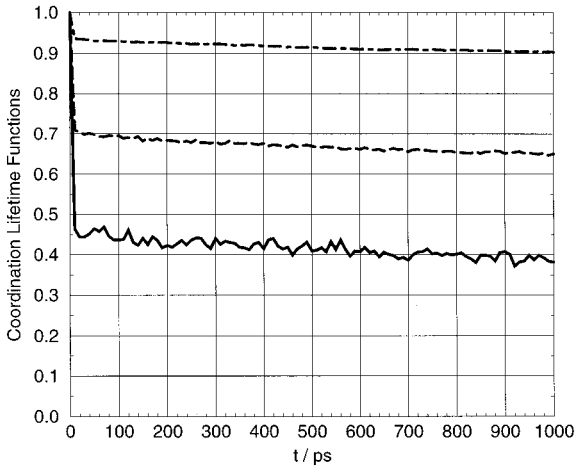

FIG. 11. Coordination lifetime functions of the three regular coordination polyhedra around Zn^{2+} ions: Tetrahedron (solid line), trigonal bipyramid (dashed line), and octahedron (dotted-dashed line).

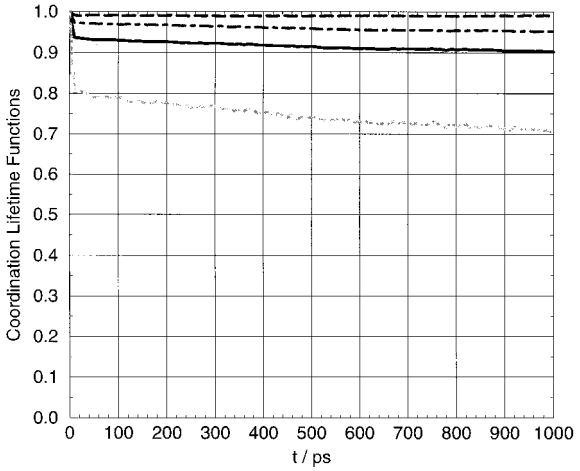

FIG. 12. Coordination lifetime functions of octahedra in general (solid line) and the three important octahedral subspecies (one Br^- and five O, long-dashed line; two Br^- and four O, dotted-dashed line; three Br^- and three O, dashed line), in particular.

B. Dynamic coordination

In light of the rather high content of regular polyhedra in the first coordination shells around Zn^{2+} ions—71% of all coordination shells are either tetrahedra, trigonal bipyramids, or octahedra—we were interested in the dynamics of the coordination of Zn^{2+}. There are two fundamental questions that we want to ask (and answer).

(1) If at some time t_0, a Zn^{2+} ion is coordinated in a specific way by Br^- ions and/or O atoms, what is the probability, that after some time t, the coordination of this Zn^{2+} ion is still the same?

(2) If at some time t_0, a Zn^{2+} ion is coordinated in a specific way by Br^- ions and/or O atoms, what is the probability, that after some time t, the Zn^{2+} ion is coordinated in a specific, different way by Br^- ions and/or O atoms?

Please note that we are not interested in the identity of the ligands coordinating a central Zn^{2+} ion, only the characteristics of the coordination geometry are important to us. Question (1) addresses the problem of the lifetime of a specific coordination type and the function answering this question was therefore termed (coordination) lifetime function. It is an autocorrelation function by nature. Question (2) addresses the problem of the conversion of a coordination type into another coordination type and the function answering this question is therefore called (coordination) conversion function. It is a cross correlation function by nature.

Figure 11 shows the lifetime functions for the three regular coordination types of Zn^{2+} ions in $ZnBr_2 \cdot 3H_2O$. All lifetime functions show a fast initial decay, that is dominant for about 10 ps. This suggests, that many of these polyhedra decay within the first few picoseconds. After that, all regular polyhedra are remarkably stable. Furthermore, all of the polyhedra decay at about the same rate, and this rate remains almost constant throughout the accessible time-window of about 1 ns. After about 1 ns, the probability that a Zn^{2+} ion that once was octahedrally coordinated is still octahedrally coordinated is about 0.9, the probability that a Zn^{2+} ion that once was trigonal bipyramidally coordinated is still trigonal bipyramidally coordinated is about 0.65 and the probability that a Zn^{2+} ion that once was tetrahedrally coordinated is still tetrahedrally coordinated is about 0.38.

The important thing to note is, that the dynamical behaviour of these three regular polyhedra differs almost exclusively in the short-term regime. In this short-term region, tetrahedra decay much faster than trigonal bipyramids which, in turn, decay faster than octahedra.

In Fig. 12 we see the lifetime functions for general octahedral coordination (independent of the constitution of the octahedron) and for the prominent numbers of Br^- ions in the coordinating octahedron. Both octahedra with a low number of Br^- ions (1 and 2 respectively) show an extraordinarily slow decay, whereas the octahedra with three Br^- ions and three O atoms decay much faster. It is noteworthy, that although only 7% of all Zn^{2+} ions are coordinated by an octahedron consisting of one Br^- ion and five O atoms and 27% of all Zn^{2+} ions are coordinated by an octahedron with two Br^- ions and four O atoms, the stability of the former coordination type is higher than that of the latter!

As we have now answered the question how probable the change from a particular coordination type to any other coordination type is, we are interested in the more specific question how probable the change from a particular coordination type to another particular coordination type is. Figure 13 answers this question for the conversion of coordinating tetrahedra, trigonal bipyramids, and octahedra into each other.

First of all, the conversions from octahedron to tetrahedron and vice versa—in other words those conversions that need the addition or subtraction of two ligands—are hardly detectable and consequently not included in Fig. 13. Secondly, the obviously bad statistical accuracy of the conversion function for the conversion from tetrahedron to trigonal bipyramid is due to the low number of tetrahedra in the

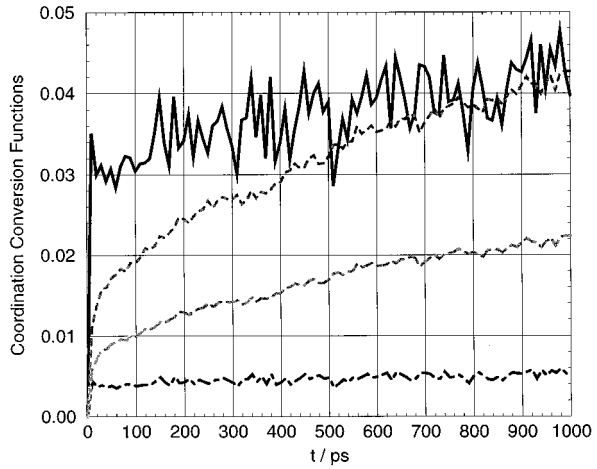

FIG. 13. Coordination conversion functions for the dominant conversions from one regular coordination polyhedron to another regular coordination polyhedron. From tetrahedron to trigonal bipyramid, solid line (top); from trigonal bipyramid to tetrahedron, dashed-dotted line (bottom); from trigonal bipyramid to octahedron, dashed line (second from top); from octahedron to trigonal bipyramid, long-dashed line (second from bottom). The conversions from octahedron to tetrahedron and vice versa are hardly detectable and therefore not included here.

system. However, this should not spoil the semiquantitative evaluation of this function.

All these conversion functions show a significantly different behaviour that ranges from a very fast initial ascend and modest subsequent slope (in the case of tetrahedron to trigonal bipyramid and trigonal bipyramid to tetrahedron) to significant long-term increases (in the case of trigonal bipyramid to octahedron and octahedron to trigonal bipyramid). This can be interpreted as follows.

(i) *Tetrahedron to trigonal bipyramid.* This conversion needs the addition of one ligand, which can obviously be accomplished very fast, since the probability of this conversion almost reaches its final value after 10 ps and does not change spectacularly as a function of time. Since the probability of decay of tetrahedra is rather high (cf. Fig. 11), the conversion of a tetrahedron to a trigonal bipyramid occurs quite often, also. However, please note, that ''often'' in this case means a probability of approximately 0.045 after an elapsed time of 1 ns. Figure 11 tells us that after this time the probability of decay of a tetrahedron is already 0.6, which means that most of the tetrahedra probably decay into an irregular, five-ligand-sized structure and not primarily into a (regular) trigonal bipyramid.

(ii) *Trigonal bipyramid to octahedron.* The prototypical trigonal bipyramid consists of three Br^- and two O, whereas the prototypical octahedron is made of two Br^- and four O. This means that the conversion from the former to the latter involves the subtraction of one Br^- and the addition of two O, which is without doubt a rather complex reaction. This complexity explains why the conversion probability for this reaction is quite small in the short-term region but increases steadily as we go towards longer time-intervals.

(iii) *Octahedron to trigonal bipyramid.* Firstly, Fig. 11 shows that octahedra are quite stable, which means that this conversion is significantly less probable than the reverse reaction just discussed. Secondly, the conversion involves the exchange of many ligands—exactly as in the case of the reverse conversion—and is therefore a complex remodeling of the first coordination shell of the involved Zn^{2+} ion. As before, the probability for such a complex conversion to occur within a short span of time is low, but it is higher for large spans of time.

(iv) *Trigonal bipyramid to tetrahedron.* As was the case for the reverse conversion, this reaction simply involves the movement of one ligand and can therefore occur fast. This is why the probability of this conversion has approximately the same value for a time interval of 10 ps as it has for a time interval of 1 ns.

IV. SUMMARY

We performed a long (2.2 ns) MD simulation of $ZnBr_2 \cdot 3H_2O$, calculated the RDF's from that simulation, and combined the RDF's using the coefficients given in Table II to reproduce the functions that were determined experimentally by Mager[21] for the same system using anomalous x-ray diffraction. The force-field parameters for the simulation were taken from an independent source, namely the general-purpose GROMOS package. Comparing these functions, we found that the MD simulation gives a structural view of $ZnBr_2 \cdot 3H_2O$ that is compatible with that given by the x-ray diffraction experiments. From this compatibility we concluded that the following, more detailed analysis of the MD simulation provides not only insight into the simulation itself but is also of relevance for the real system.

We used the Voronoi algorithm[30–32] to determine the first coordination shell around the O atoms of water and the Br^- ions. The fact that a significant number of these shells contained more than one Zn^{2+} ion gives evidence for the existence of Zn^{2+} chains that are linked by Br^- ions or O atoms, as was also found experimentally.[6,15,16,21] We did not investigate the length of these chains.

To get a better understanding of the coordination of the Zn^{2+} ions, which are the main coordinating particles in $ZnBr_2 \cdot 3H_2O$, we applied the Voronoi algorithm to determine the first coordination shell around Zn^{2+} ions. We found that on average, 45% of all Zn^{2+} ions are octahedrally coordinated by O atoms or Br^- ions, whereas only 23% are coordinated in the geometry of a trigonal bipyramid and 3% are coordinated tetrahedrally. This is in accordance with some experiments,[6,8] but in contrast to other experimental studies that found the tetrahedral coordination of Zn^{2+} ions to be prominent.[6,8–16,21] The trigonal bipyramid was not reported in the experimental literature. Regarding the exact composition of the first coordination shell around tetrahedrally coordinated Zn^{2+} ions, we found a high percentage of Br^- ions (three or four) to be dominant. This is supported by experiments[1–9]—including that of Mager[21]—but contradicted by other experimental studies.[2,10–13]

The dynamics of the coordination geometry of Zn^{2+} ions was not investigated experimentally. In the simulation we found all regular coordination geometries remarkably stable, with the octahedron being the most stable of all (after 1 ns only 10% of all octahedrons had decayed). This stability of coordination geometries is in accordance with the experimentalists view of $ZnBr_2 \cdot 3H_2O$ as a quasicrystalline system.[2–5] Regarding the conversion of the regular coordination geometries into each other, we observed three kinds of behavior. Firstly, the fast conversion from tetrahedron to trigonal bipyramid and back, which is characterized by a simple conversion mechanism. The probabilities for these conversions reach there final value after approximately 10 ps and remain essentially constant for longer spans of time. Secondly, the slow conversion from trigonal bipyramid to octahedron and back, which is characterized by a complex, concerted conversion mechanism. The probabilities for these conversions increase steadily with the elapsed time. Finally, the conversion from tetrahedron to octahedron and back, which are hardly *detectable* in the simulation.

ACKNOWLEDGMENT

This work was funded by the Austrian ''Fonds zur Förderung der wissenschaftlichen Forschung'' under Project No. P10095-CHE.

[1] W. Grzybkowski and G. Atkinson, J. Chem. Eng. Data **32**, 309 (1986).
[2] R. H. Stokes, Trans. Faraday Soc. **44**, 295 (1948).
[3] R. H. Stokes and J. M. Stokes, Trans. Faraday Soc. **41**, 688 (1945).
[4] R. H. Stokes, J. M. Stokes, and R. A. Robinson, Trans. Faraday Soc. **40**, 533 (1944).
[5] R. H. Stokes and R. A. Robinson, J. Am. Chem. Soc. **70**, 1870 (1948).
[6] T. Yamaguchi, S. Hayashi, and H. Ohtaki, J. Phys. Chem. **93**, 2620 (1989).
[7] H. Kanno and J. Hiraishi, J. Raman Spectrosc. **9**, 85 (1980).
[8] E. Kalman, I. Serke, G. Palinkas, G. Johansson, G. Kabisch, M. Maeda, and Z. Ohtaki, Z. Naturforsch. A **38**, 85 (1983).
[9] P. L. Goggin, G. Johansson, M. Maeda, and H. Wakita, Acta Chem. Scand. A **38**, 625 (1984).
[10] D. L. Wertz, R. M. Lawrence, and R. F. Kruh, J. Chem. Phys. **43**, 2163 (1965).
[11] J. P. Dreier, Ph.D. thesis, Universität Kiel, 1986.
[12] P. Dreier and P. Rabe, Rev. Sci. Instrum. **57**, 214 (1986).
[13] B. Brehler, Fortschr. Mineral. **39**, 338 (1961).
[14] W. Yellin and R. A. Plane, J. Am. Chem. Soc. **83**, 2448 (1961).
[15] K. F. Ludwig, W. K. Warburton, and A. Fontaine, J. Chem. Phys. **87**, 620 (1987).
[16] P. Lagarde, A. Fontaine, D. Raoux, A. Sadoc, and P. Migliardo, J. Chem. Phys. **72**, 3061 (1980).
[17] T. Yamaguchi, H. Ohtaki, E. Spohr, G. Palinkas, K. Heinzinger, and M. Probst, Z. Naturforsch. **41a**, 1175 (1986).
[18] M. Probst, E. Spohr, and K. Heinzinger, Chem. Phys. Lett. **161**, 405 (1989).
[19] M. Probst, E. Spohr, K. Heinzinger, and P. Bopp, Mol. Sim. **7**, 43 (1991).
[20] P. Bopp, I. Okada, H. Ohtaki, and K. Heinzinger, Z. Naturforsch. **40a**, 116 (1985).
[21] T. Mager, Ph.D. thesis, Universität Würzburg, 1991.
[22] M. P. Allen and D. J. Tildesley, *Computer Simulation of Liquids* (Clarendon, Oxford, 1987).
[23] H. J. C. Berendsen, J. P. M. Postma, W. F. van Gunsteren, and J. Hermans, *Intermolecular Forces* (Reidel, Dordrecht, 1981), p. 331.
[24] H. J. C. Berendsen, J. P. M. Postma, A. DiNola, and J. R. Haak, J. Chem. Phys. **81**, 3684 (1984).
[25] G. Löffler, H. Schreiber, and Steinhauser (unpublished).
[26] P. P. Ewald, Ann. Phys. **64**, 253 (1921).
[27] D. J. Adam and G. S. Dubey, J. Comput. Phys. **72**, 156 (1987).
[28] S. W. de Leeuw, J. W. Perram, and E. R. Smith, Proc. R. Soc. London, Ser. A **373**, 27 (1980).
[29] W. F. van Gunsteren and H. J. C. Berendsen, *GROningen MOlecular Simulation (GROMOS) Library Manual* (Biomos, Groningen, The Netherlands, 1987).
[30] G. F. Voronoi, J. Reine Angew. Math. **134**, 198 (1908).
[31] M. Neumann, F. J. Vesely, O. Steinhauser, and P. Schuster, Mol. Phys. **37**, 1725 (1979).
[32] J. D. Bernal and S. V. King, *Physics of Simple Liquids* (North Holland, Amsterdam, 1968).